An International Journal of Optimization and Control: Theories & Applications
ISSN: 2146-0957 eISSN: 2146-5703
Vol.15, No.4, pp.649-669 (2025)
https://doi.org/10.36922/IJOCTA025170086

RESEARCH ARTICLE

Rolling bearing fault diagnosis method based on GJO–VMD, multiscale fuzzy entropy, and GSABO–BP neural network

Jingsong Zhang[1†], Xiaolong Zhou[2†], Soo Siang Yang[1*], Min Keng Tan[1], Yanzhen Wang[2], Bin Zheng[1], Jing Zhe[2], and Haoyu Li[2]

[1]Faculty of Engineering, Universiti Malaysia Sabah, Kota Kinabalu, Sabah, Malaysia
[2]College of Mechanical Engineering, Beihua University, Jilin, Jilin, China
zhangjingsong851@gmail.com, xlzhou1987@163.com, ssyang@ums.edu.my, tanminkeng@ums.edu.my, wyz200012051@163.com, binz74609@gmail.com, jingzhe20041004@163.com, Lihaoyu030722@163.com

ARTICLE INFO

Article History:
Received: April 21, 2025
1st revised: May 22, 2025
2nd revised: June 9, 2025
Accepted: June 9, 2025
Published Online: August 11, 2025

Keywords:
Rolling bearing
Fault diagnosis
Variational mode decomposition
Golden jackal optimization
Multiscale fuzzy entropy
Golden sine subtraction-average-based optimizer–back-propagation neural network

ABSTRACT

Accurate fault diagnosis of rolling bearings is hindered by the weak nature of early fault signals and the limited availability of labeled data, especially under small-sample conditions. To overcome these challenges, this paper proposes a novel method combining golden jackal optimization (GJO) with improved variational mode decomposition (VMD), enhanced feature extraction, and optimized classification. First, GJO is used to optimally determine the key decomposition parameters of VMD, thereby improving the accuracy of vibration signal decomposition. A comprehensive discrimination factor algorithm then selects fault-sensitive intrinsic mode functions, and the signal is reconstructed to enhance fault characteristics. Multiscale fuzzy entropy is calculated from the reconstructed signals at multiple scales to build distinct state feature vectors. These vectors are fed into a back-propagation neural network optimized via the golden sine subtraction-average-based optimizer for precise fault classification. The method's effectiveness is verified through simulation and experimental data. Compared with conventional approaches, it shows superior performance in extracting weak fault features and maintaining high diagnostic accuracy under small-sample scenarios. This integrated framework presents a robust solution for rolling bearing fault diagnosis.

1. Introduction

Rolling bearings used in today's machinery are essential components, especially for rotating machines such as motors, automobiles, and aircraft.[1,2] As key load-bearing elements, the operational status of rolling bearings has a direct impact on the performance and service life of the machinery. Failure in these bearings can lead to a decline in equipment performance, increased energy consumption, and even severe mechanical failures or safety incidents.[3,4] Therefore, research on rolling bearing fault diagnosis is not only theoretically significant but also highly valuable in practical engineering applications. Recurring faults in rolling bearings include fatigue spalling and localized damage on inner/outer rolling elements. The mechanical system generates abnormal vibration signals when a bearing failure occurs, carrying critical information that reflects fault characteristics.[5] The extraction of fault features from complex vibration signals and their accurate fault diagnosis and prognostics have become a hot research topic. The vibration signal analyses can

[†] *These authors contributed equally to this work.*
*Corresponding Author

be used for the exact identification of fault features of rolling bearings.

Traditional signal processing methods, such as the Fourier transform[6] and wavelet transform,[7] are effective in extracting frequency-domain characteristics of fault signals. However, these methods have limitations when dealing with nonlinear, non-stationary signals and lack adaptability.[8] Consequently, researchers have developed new signal processing methods, such as empirical mode decomposition (EMD)[9] and ensemble EMD (EEMD),[10] and have achieved certain successes. For example, Zhou et al.[11] employed EMD to filter noise from signals and selected sensitive intrinsic mode functions (IMFs) for reconstruction, achieving fault diagnosis of the bearing's inner race. Yao et al.[12] applied EMD with an auto-regression model (AR) spectrum analysis for bearing fault diagnosis. Likewise, Qin et al.[13] developed dynamic models for different bearing faults and extracted joint time–frequency entropy features from EMD-decomposed signals for fault classification using machine learning techniques. Zhang et al.[14] proposed a new method using EEMD and box dimension analysis, where denoised signals are decomposed, and relevant features are used in a probabilistic neural network for fault identification. Similarly, Damine et al.[15] applied a kurtosis-based median absolute deviation method to directly identify sensitive IMF components, demonstrating the effectiveness of this approach for bearing fault detection.

The performance of these methods in processing nonlinear, non-stationary signals has also been established. EMD suffers from mode-mixing issues, while EEMD, though able to mitigate these issues, introduces white noise that requires extensive averaging, impacting decomposition accuracy.[16] To address these issues, variational mode decomposition (VMD),[17] the adaptive signal decomposition method, has arisen as a prominent technique. VMD decomposes complex signals into a series of IMFs while effectively avoiding mode mixing and providing good frequency resolution. Since its introduction, VMD has been widely applied in rolling bearing fault diagnosis.

The choice of the decomposition number (K) and the quadratic penalty parameter (α) has a strong effect on the decomposition performance of VMD, which significantly influences the results. Relying on empirical or prior knowledge to set these parameters may lead to inaccurate decomposition, reducing VMD's efficiency and ignoring the interrelationship between parameters. Researchers have explored intelligent optimization algorithms, such as the grey wolf optimizer (GWO),[18] the grasshopper optimization algorithm,[19] and cuckoo search,[20] to determine optimal values for K and α. Among these, golden jackal optimization (GJO)[21] has demonstrated faster convergence and a stronger ability to avoid local optima, making it more suitable for optimizing VMD parameters for better decomposition outcomes.

However, despite the effectiveness of signal decomposition and reconstruction, capturing fault characteristics under complex operating conditions remains challenging. Entropy measures, such as multiscale fuzzy entropy (MFE), effectively quantify signal regularity and detect subtle changes, offering advantages like reduced sensitivity to parameter variations and high convergence accuracy.[22] This makes MFE capable of distinguishing different fault types. Therefore, in the field of rotating machinery fault diagnosis, it is often used as a signal feature for fault pattern recognition.[1]

To further enhance diagnostic accuracy, effective classification models are needed for different types of bearing faults. The back-propagation (BP) neural network,[23] a classic machine learning algorithm, is widely applied in fault classification. It minimizes error by adjusting weights and biases and mapping input data nonlinearly. However, traditional BP networks are prone to local minima and sensitive to initial parameters, reducing classification performance. To overcome this, a hybrid optimization approach combining GWO and simulated annealing, termed the golden sine subtraction-average-based optimizer (GSABO), is introduced. GSABO effectively optimizes BP neural network parameters, avoiding local minima and improving classification accuracy and stability.

Aiming at the challenge of effectively extracting early fault characteristics of rolling bearings and achieving reliable diagnosis results with small samples, this paper proposes a novel fault diagnosis method. The signal feature information is extracted using VMD combined with MFE, while the fault-diagnosis result is achieved using a GSABO–BP neural network. The major contributions of this paper, compared to existing methods, are the following:

(i) The GJO algorithm is employed to jointly optimize the two key decomposition parameters of VMD—K and α. This approach effectively eliminates the reliance on manual parameter selection, which

typically demands extensive prior experience and incurs high computational costs, thereby reducing the influence of human subjectivity. Moreover, by integrating a comprehensive evaluation factor method, the IMFs' features that are most sensitive to signals can be reliably selected, ensuring the accuracy of subsequent feature extraction.

(ii) The MFE is capable of capturing the complexity of a signal across multiple scales by computing its fuzzy entropy at each scale. When applied to VMD-reconstructed signals, MFE benefits from the effective suppression of noise and irrelevant components, enhancing the precision of entropy calculation. The integration of VMD and MFE thus significantly improves the robustness and accuracy of signal feature extraction.

(iii) The MFE values computed at designated scale factors are used as quantitative feature parameters and are subsequently input into a Bo–XGBoost classification model. This hybrid framework enables accurate classification of rolling bearing fault types. Compared with conventional fault classification models and signal decomposition techniques, the proposed method demonstrates superior diagnostic performance, even under small-sample conditions.

In the following section, the basic theory is explained in Section 2, the framework of the proposed method is provided in Section 3, and Section 4 validates the performance of the GJO–VMD in signal decomposition and correct selection of IMF components using the evaluation factor algorithm. In Section 5, the proposed method is further applied in a real-world rolling bearing fault detection application. To conclude the study, in Section 6, the main findings are summarized.

2. Basic theory

2.1. Variational mode decomposition algorithm

The VMD algorithm models the signal as a variational problem and iteratively updates each component to obtain an optimal solution, extending the classic Wiener filter to multiple adaptive bands. The signal is decomposed into IMF components with different center frequencies and bandwidths, iteratively repeating the center frequency and bandwidth for each modal component, thereby facilitating adaptation. For more information, please refer to the article by Dragomiretskiy and Zosso.[17]

2.2. Selection of key decomposition parameters for variational mode decomposition based on golden jackal optimization

Based on the social interaction behavior and hunting behavior of golden jackals, a population intelligence optimization method, GJO (also known as Asian jackals), has been derived. The algorithm mimics the process of individuals working together and competing to discover the best answer during golden jackals' eating and hunting activities. The article by Chopra and Ansari[21] provides a thorough description of the theory of GJO.

2.2.1. Determining the fitness function

The fitness function plays a critical role in guiding the parameter optimization process of the VMD algorithm through artificial intelligence-based search algorithms. This function measures the effectiveness of the VMD in the current parameter settings and subsequently updates the parameters based on these results to enhance overall effectiveness. Envelope entropy evaluates the degree of disorder in the signal and effectively reflects the proportion of random components. A higher envelope entropy indicates a greater presence of random components, while a lower envelope entropy suggests a more ordered signal structure.[24]

In the case of rolling bearing faults, periodic impacts generated by faults make the signal more orderly, leading to a reduction in envelope entropy. Compared to other fitness functions, envelope entropy is an optimal choice due to its stronger global search capability and robustness, making it better suited to adapt to complex and changing environments while also offering higher optimization efficiency.[25] The envelope entropy is determined to be the fitness function in this study, as it not only ensures the proper combination of VMD parameters to achieve fidelity and reliability of the decomposition results but also enhances the robustness of the algorithm.

$$E(m) = -\sum_{m=1}^{M} [p_n(n) \log 2p_n(m)] \tag{1}$$

$$p_n(m) = a_n(m) / \sum_{m=1}^{M} a_n(m) \tag{2}$$

In this context, n represents the IMF component index; m represents the index of the equal-length interval used in calculating the envelope entropy; $p_n(m)$ is the probability of the n-th IMF component falling within the m-th equal-length interval; and $a_n(m)$ is the count of points from the n-th IMF component within the m-th interval.

The steps for optimizing VMD using the GJO algorithm are as follows:

a. Initialize GJO parameters: Begin by setting the parameters for the GJO algorithm and defining the range for the VMD parameters K and α.

b. Calculate fitness values: Assess the suitability of every member within the group. The two jackals are selected among the elite as the best-fit individuals with the highest fitness, serving as both the jackal pair and the prey.

c. Update prey position through exploration, encirclement, and attack: The golden jackals update the prey's position by exploring and approaching it, surrounding it, stimulating it, and finally attacking it.

d. Replace individuals based on prey position updates: Update the positions of the best and second-best individuals by replacing them with the positions of the current prey.

e. Repeat Steps b–d: Iterate the process until the maximum number of cycles is reached. Should the termination criterion be met, the algorithm outputs the optimal parameter combination $[K, \alpha]$. If the expected optimal effect is not achieved, the process returns to Step b and repeats the whole process until the preset termination conditions are met. This procedure allows for an effective optimization of VMD parameters by leveraging the cooperative and competitive dynamics within the GJO framework.

Figure 1 illustrates the key parameters of the VMD algorithm employing the GJO method.

2.3. Sensitive intrinsic-mode-function selection algorithm based on comprehensive evaluation factors

Effectively identifying informative components from the IMF decomposition of VMD is critical for the efficacy of signal processing. Conventional methods for excluding and reconstructing false IMFs often fall short, particularly when analyses are confined to either the time domain or the frequency domain alone. Such approaches tend to overlook the signal's combined time–frequency attributes, leading to the loss of critical information. To rectify this deficiency, this study presents a comprehensive evaluation factor-based algorithm for identifying sensitive IMF components.[26]

The correlation coefficient is an effective metric for assessing the similarity between signals. Therefore, computing the correlation coefficient in the frequency domain can effectively suppress noise interference and improve calculation accuracy. In addition, frequency-domain analysis reveals the characteristics of signals across different frequencies, providing richer information for signal processing and feature extraction. Moreover, when a rolling bearing experiences a fault, the probability density of high-amplitude vibrations increases, causing the amplitude distribution to deviate from a normal distribution. This results in skewness or dispersion in the normal curve and an increase in kurtosis.

To identify sensitive components that effectively represent signal characteristics, this study computed both the frequency-domain cross-correlation coefficients and the kurtosis for each mode component resulting from VMD. By applying a weighted factor to these values, the IMFs that optimally capture the signal's key features were selected. This method provides a more robust approach to IMF selection, ensuring that important diagnostic information is retained.

Under the action of the Coati Optimization Algorithm (COA)–VMD, the vibration signal of the rolling bearing $(x[t], t = 1, 2, \ldots, n)$ is decomposed into IMF components $(K; u_i[t], i = 1, 2, \ldots, K)$. The global criterion function constitutes the kernel of the sensitive IMF discrimination algorithm, enabling accurate computation.

(i) Compute the frequency-domain cross-correlation coefficient (ρ) for each IMF component relative to the original signal.

$$\rho_i = \frac{\int_0^{f_a} (G_{u_i} - \bar{G}_u)(G_{x_i} - \bar{G}_x) df}{\sqrt{\int_0^{f_a} (G_{u_i} - \bar{G}_u)^2 df} \cdot \sqrt{\int_0^{f_a} (G_{x_i} - \bar{G}_x)^2 df}} \tag{3}$$

In this equation, G_u and G_x represent signal power spectra $u_i(t)$ and $x(t)$, respectively; $\overline{G}_u$ and $\overline{G}_x$ denote the corresponding mean power spectra; and f_a indicates the analysis frequency.

(ii) Calculate the kurtosis of each IMF component:

$$kur_i = \frac{E[u_i(t) - \bar{u}(t)]^4}{\sigma^4} \tag{4}$$

In the given equation, $\bar{u}(t)$ and σ represent the mean values of the i-th IMF

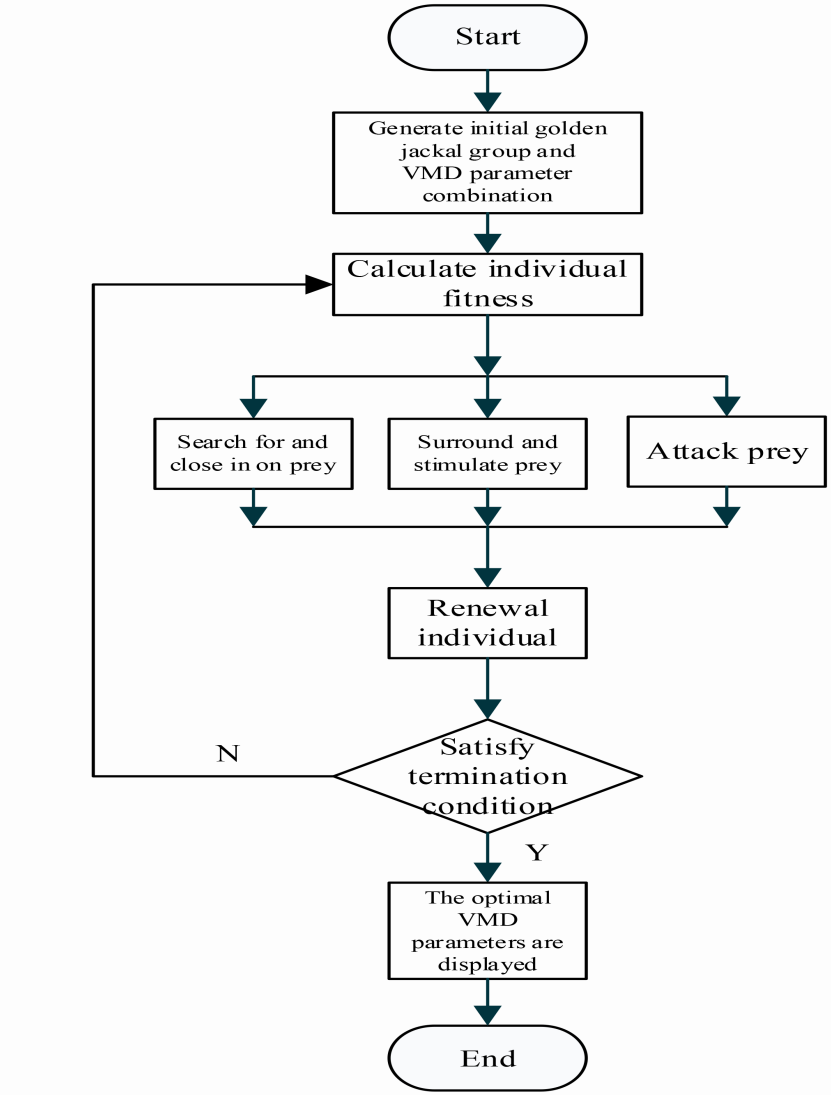

Figure 1. A flowchart illustrating the optimization of key parameters of variational mode decomposition (VMD) using the golden jackal optimization

component, where $E[]$ represents the anticipated value of the variable.

(iii) Use the subsequent formula to compute the time–frequency domain weighting value λ_i:

$$\lambda_i = \beta \cdot e_i + \gamma \cdot kur_i \tag{5}$$

In this equation, β and γ serve as weighting coefficients, subject to the constraint that their sum equals. Given that the signal's representation in the frequency domain is more resistant to noise and various disturbances, it was set that $\beta = 0.6$ and $\gamma = 0.4$.

(iv) Calculate the comprehensive evaluation factor (δ_i):

$$\delta_i = \frac{\lambda_i - \min(\lambda)}{\max(\lambda) - \min(\lambda)} \tag{6}$$

(v) Compute the overall assessment factor (δ_i) to reorder the weights of the time–frequency domain of each subcarrier in descending sequence and form a vector ($\{\delta\} = \{\delta_1, \delta_2, \ldots, \delta_K\}$).

(vi) Measure how far off the complete evaluation criteria are between adjacent components.

$$d_i = \delta_i - \delta_{i+1} \tag{7}$$

(vii) The largest dissimilarity index (m) should be defined. The first m entries of the reordered set ($\{\delta\}$) under the comprehensive judgment criterion represent the sensitive mode fragments conveying the primary data information of the signal.

The invention relates to an efficient algorithm, which is specially used for distinguishing and identifying IMF components. The algorithm

is based on the evaluation criteria in the time–frequency domain, and its core is to ensure that the unique characteristics of each IMF component are fully reflected and identified in the time domain. At the same time, the algorithm also takes into account the relationship between these components and the original signal in the frequency domain, thus ensuring the comprehensiveness and accuracy of the analysis. Through this method, a complex signal can be effectively decomposed into a series of IMF components with physical significance, providing a more accurate tool for signal processing and analysis.

This procedure enhances the discrimination by mitigating any impact of the interfering factors and facilitating the identification of spurious IMF components that do not embed fault information. Additionally, it mitigates the impacts of unrelated modal components on fault information and minimizes the influence of human factors associated with the setting of threshold values, thereby enhancing the accuracy of fault feature extraction.

2.4. Multiscale fuzzy entropy algorithm

By mapping the original signal into a high-dimensional space, describing the signal's complexity using high-dimensional vectors within the amplitude tolerance, and defining the similarity between the signals using a fuzzy function, fuzzy entropy produces more accurate and realistic computation results. Nevertheless, the conventional fuzzy entropy only uses one scale to describe the signal complexity, which could result in the loss of crucial signal information and compromise the precision of fault feature extraction. By extracting the signal's fuzzy entropy value from several scales, MFE can more thoroughly capture the signal's characteristic information, increasing the precision of defect diagnosis.[22]

The specific calculation process of MFE is as follows[22]:

Coarse-graining of the original sequence. For the original time series ($X_i = \{x_1, x_2, ..., x_N\}$) of length N, under the condition that the embedding dimension (m) and the similarity tolerance (r) are given in advance, the coarse-grained processing of the series is carried out. The new coarse-grained vector is:

$$yj(\tau) = \frac{1}{\tau} \sum_{i=(j-1)\tau=1}^{j\tau} x_i, 1 \le j \le \frac{N}{\tau} \qquad (8)$$

Let τ denotes the scale factor. When $\tau = 1$, $y_j(1)$ represents the original time series. For non-zero values of τ, the original sequence is segmented into coarse-grained vectors $y_j(\tau)$, each with a length of N/τ.

The fuzzy entropy of the sequence is then computed at each scale τ, and the resulting values are referred to as the MFE.

$$MFE(x, \tau, m, n, r, N) = FuzzyEn(y^\tau, m, n, r, N^\tau) \qquad (9)$$

Due to the high complexity of vibration signals in rotating machinery and the diversity of fault types, a single-scale fuzzy entropy is insufficient to capture the full extent of the fault-related information. The complexity and richness of fault characteristics cannot be effectively represented at a single scale, leading to incomplete feature extraction. Therefore, this study employs MFE as the method for signal feature extraction.[27] By analyzing the signal over multiple scales, MFE effectively overcomes the limitations of single-scale approaches and provides a more comprehensive characterization of the signal complexity under various operating conditions.

2.5. Golden sine subtraction-average-based optimizer–back-propagation neural network

2.5.1. Subtraction-average-based optimizer algorithm

An intelligent optimization technique based on mathematical principles is the subtraction-average-based optimizer (SABO) algorithm. Its fundamental idea is that the subtraction average of the group members is responsible for updating the locations of fellow group members within the search space. In addition to reducing reliance on a particular candidate, the algorithm successfully avoids settling into local optima, enhancing its global search capability and optimization effectiveness.[28]

2.5.2. Golden sine subtraction-average-based optimizer

The SABO algorithm updates particle positions using the subtraction average method. To avoid getting trapped in local optima, this study enhanced the SABO algorithm by leveraging the advantages of the golden sine algorithm in global optimization. In instances where the fitness values of particles were stable across iterations in the SABO algorithm, the golden sine algorithm is invoked to adjust particle positions. The precise

formula utilized by the chosen golden sine operator is delineated as follows:

$$X_i(t+1) = X_i(t)\,|\sin R_1| + R_2 \sin(R_1)\,|\,aX_{best} - bX_i(t) \tag{10}$$

In this context, R_1 is a random number ranging from 0 to 2π, which determines the step size for updating the position of individual i in the next generation; R_2 is a random number ranging from 0 to π, which dictates the direction of the next update for individual i; and the parameters a and b are the golden section coefficients that influence the search space of the particles, facilitating a more optimal selection that guides the particles toward superior values. The formula for the calculation is presented as follows:

$$\begin{cases} a = -\pi(1-\tau) + \pi\tau \\ b = -\pi\tau + \pi(1-\tau) \end{cases} \tag{11}$$

In this equation, τ represents the golden ratio, with a value of $\frac{\sqrt{5}-1}{2}$.

The GSABO is the outcome of combining the golden sine and SABO. Every time an iteration occurs, all particles' positions and velocities are updated, and the objective function values for their new locations are computed. Each particle's individual best location is updated by comparing these new values with the previously saved individual best values. In the end, the algorithm determines which particle is in the optimal place globally.

2.5.3. Back-propagation neural network

The fundamental attributes of the BP neural network encompass the forward propagation of signals and the subsequent back propagation of errors, defining its structure as a multilayer feedforward neural network. The network uses a nonlinear transformation of the activation function and a weighted summation of the input data to generate an output signal. When the actual output deviates from the expected output, the error backpropagation process is triggered. During this process, the algorithm adjusts the weights and thresholds to minimize the error, thereby improving the model's acuracy.[23]

2.5.4. Golden sine subtraction-average-based optimizer–back-propagation neural network

The selection of an appropriate fitness function is crucial for optimizing the parameters of the BP neural network through the application of artificial intelligence search methods. This function allows for parameter adjustments targeted at improving overall performance by quantifying the BP neural network's performance under the present parameter configuration. In order to balance training and generalization to improve model resilience, the fitness function in this study was defined as the sum of the recognition error rates on the training set and the test set. The following is the definition of the fitness function:

$$F = TrE + TeE \tag{12}$$

In the equation, TrE and TeE represent the recognition error rates of the training and testing sets, respectively.

The steps for optimizing the BP neural network with the GSABO algorithm are as follows (Figure 2):

- Step 1: Set the initial weight, threshold, and parameters of the GSABO algorithm of the BP neural network.
- Step 2: Calculate the fitness value for each particle.
- Step 3: Check to determine whether the fitness has altered. If a change occurs, update the particle's position immediately; if not, apply the golden sine method.
- Step 4: Modify the BP neural network's parameters.
- Step 5: Check if the maximum iteration stopping condition is met. If it is met, output the optimal parameters. If not, revert to Step 2 for additional iterations, continuing this process until the termination criteria are met.

3. Fault diagnosis method based on GJO–VMD, MFE, and GSABO–BP neural network

The steps of the proposed fault diagnosis method are as follows (Figure 3):

- Step 1: Utilize a rolling fault simulation test bench to acquire vibration signals from rolling bearings across varying operational conditions.
- Step 2: Utilize the envelope entropy as a fitness criterion. The VMD method has been improved with the GJO algorithm. The fault signal is then subjected to decomposition into a series of IMFs by implementing VMD with these optimized parameters.
- Step 3: Apply a fine-grained IMF part separation algorithm, which is built on a comprehensive judgment index in the time–frequency domain. This step identifies the IMF components that are sensitive to signal characteristic information, and these components are then used to reconstruct the signal.

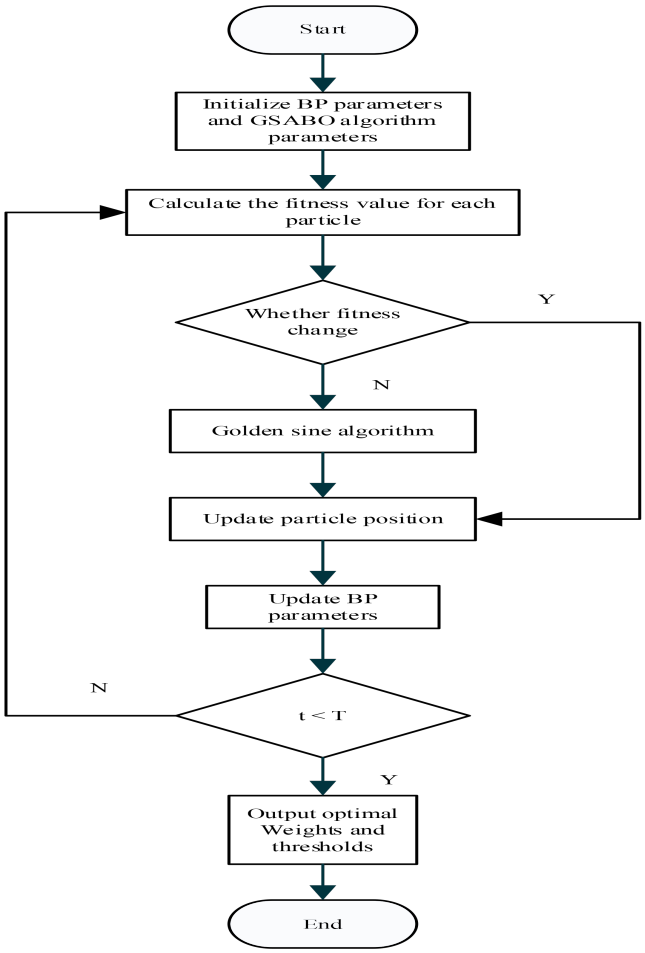

Figure 2. A flowchart illustrating the golden sine subtraction-average-based optimizer (GSABO)–back-propagation (BP) neural network

- Step 4: MFE is used to extract features from reconstructed signals and construct feature sets representing different states.
- Step 5: With the state feature set learned in Step 4, the GSABO–BP neural network classifier can be guided during the classification process. This structured approach enhances fault diagnosis accuracy by leveraging the strengths of the GJO for parameter optimization, VMD for signal decomposition, MFE for feature extraction, and GSABO–BP neural network for feature classification.

4. Simulation analysis

To validate the effectiveness of the VMD method, an early fault signal for rolling bearings was established, as shown in Equation (13):

$$\begin{cases} y(t) = x(t) + n(t) \\ x(t) = \sum_i e^{-2\pi f_n g t_0} \cdot A_0 \sin[2\pi f_n \sqrt{(1-g^2)} \cdot t_0] \end{cases} \tag{13}$$

where $n(t)$ is Gaussian white noise, and $x(t)$ is the periodic impact signal produced by rolling bearing failures. The following are the parameters: sampling frequency fs = 1200 Hz, number of sample points N = 6000, fault impact duration T = 0.01 s, fault characteristic frequency f = $1/T$ = 100 Hz, natural frequency f_n = 3000 Hz, displacement constant A_0 = 5, and damping coefficient g = 0.1.

Figure 4 illustrates the simulated signal's time-domain waveform. The noise obscures the rolling bearing's periodic impact characteristics, inevitably diminishing the accuracy of the subsequent signal feature extraction process.

The most popular and user-friendly technique for diagnosing rolling bearing faults is the envelope spectrum approach. Figure 5 presents the envelope spectrum obtained from the simulated signal.

In order to diagnose the rolling bearing fault, the simulated signal *y(t)* must be processed to remove interference components and enhance the accuracy of fault feature extraction. As illustrated in Figure 5, background noise causes the spectral line at the fault characteristic frequency in the envelope spectrum to be less prominent. With significant interference present, identifying

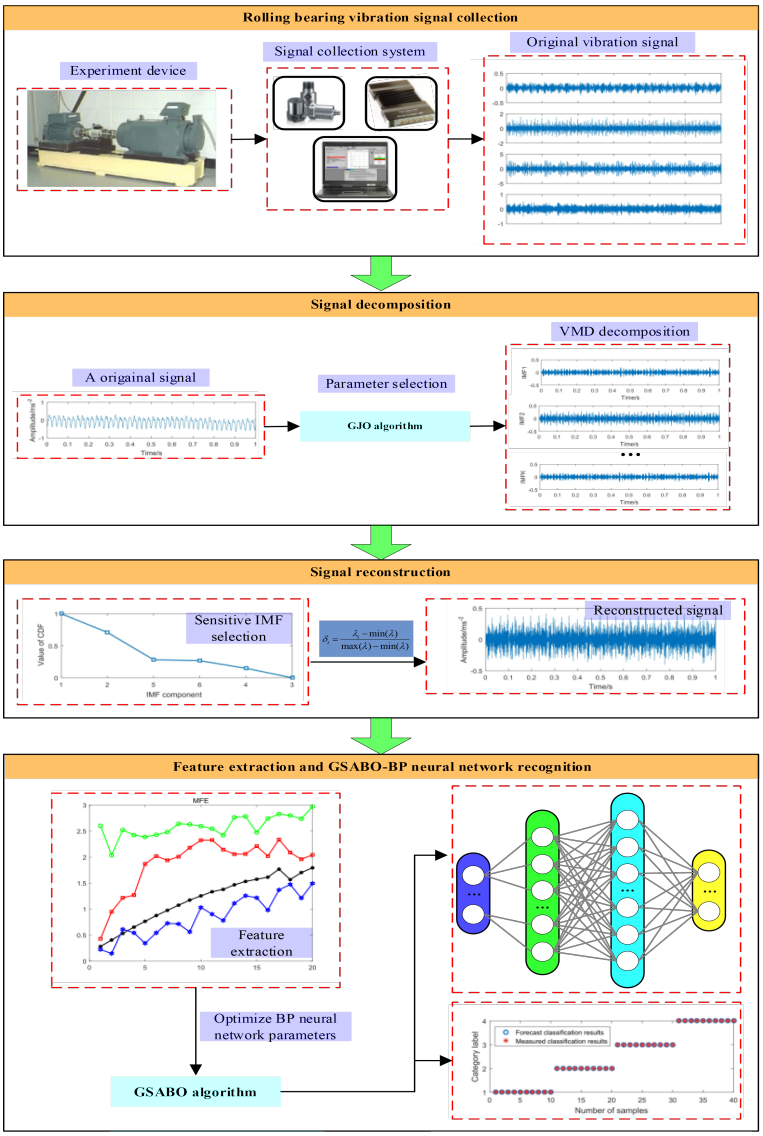

Figure 3. A flowchart illustrating the steps in the proposed fault diagnosis method
Abbreviations: BP: Back propagation; GJO: Golden jackal optimization; GSABO: Golden sine subtraction-average-based optimizer; IMF: Intrinsic mode functions; VMD: Variational mode decomposition.

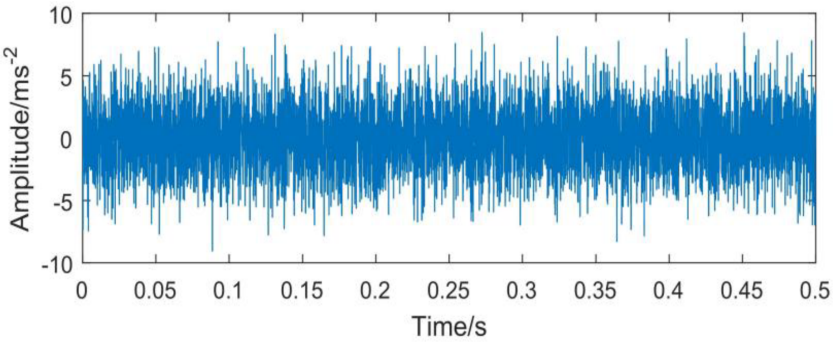

Figure 4. Time-domain waveform of the simulated signal $y(t)$

the fault characteristic frequency proved challenging. Therefore, the VMD method was employed to decompose the aforementioned signal.[29]

During the VMD decomposition process, the key parameters—K and α—were optimized using the GJO algorithm. Specifically, the search range for K was set to [2, 7], and for α, it is set to [100, 5000]. Envelope entropy was adopted as the fitness function to guide the optimization of both parameters.

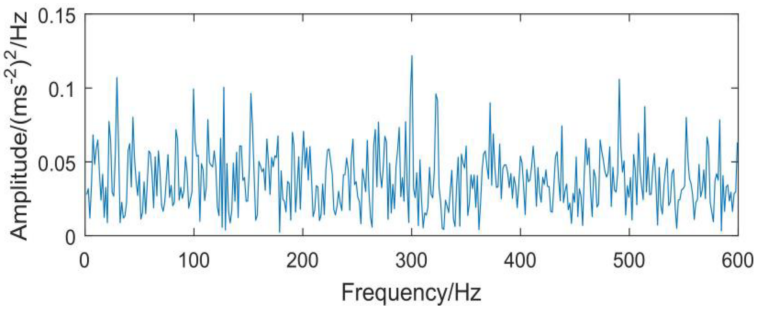

Figure 5. Envelope spectrum of the simulated signal $y(t)$

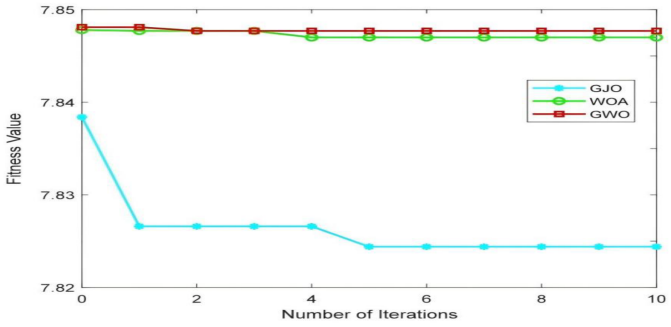

Figure 6. Fitness iteration curve
Abbreviations: GJO: Golden jackal optimization; GWO: Grey wolf optimizer; WOA: Whale optimization algorithm.

To demonstrate the superior search performance of GJO, two other algorithms—GWO and whale optimization algorithm (WOA)—were employed for comparative analysis. In the experiments, the population size for each optimization algorithm was set to 50, and the maximum number of iterations was fixed at 10. Each algorithm was applied to optimize the VMD parameters for the simulated signal shown in Figure 4. The corresponding fitness convergence curves and optimization results are presented in Figure 6 and Table 1.

Table 1. Optimization results of variational mode decomposition parameters using different algorithms

Intelligent search algorithms	**[K, α]**	**Fitness value**
GJO	[6, 2922]	7.82522
GWO	[5, 1748]	7.84541
WOA	[6, 4000]	7.84544

Abbreviations: GJO: Golden jackal optimization; GWO: Grey wolf optimizer; WOA: Whale optimization algorithm.

As shown in Figure 6, with the increase in the number of iterations, the fitness value gradually decreases, indicating that the decomposition results are steadily approaching an optimal solution under the guidance of optimized parameters. The stabilization of the fitness curve further confirms that the optimal parameter values have been successfully identified. Although the GWO and WOA algorithms demonstrate relatively fast convergence speeds, their fitness values remain significantly higher than those obtained by the GJO algorithm. As evidenced in Table 1, the GJO algorithm achieves the best fitness value, highlighting its superior capability in accurately determining optimal decomposition parameters. Therefore, the VMD parameters optimized using GJO were applied to decompose the simulated signal shown in Figure 4. The resulting time-domain waveform and frequency spectra of the extracted IMF components are presented in Figure 7.

With each IMF component's frequency dispersed from low to high frequencies and each component focused around its center frequency, the signal decomposition findings are reasonable, as illustrated in Figure 7. There is no discernible frequency overlap, suggesting that modal aliasing is not present. The total evaluation factor for each IMF component is computed, as illustrated in Figure 8, to effectively choose the IMF components that are sensitive to signal characteristics.

As shown in Figure 8, it is easy to identify that IMF4 and IMF2 have the largest difference. Therefore, IMF4 was chosen as the sensitive IMF component for envelope demodulation. Figure 9

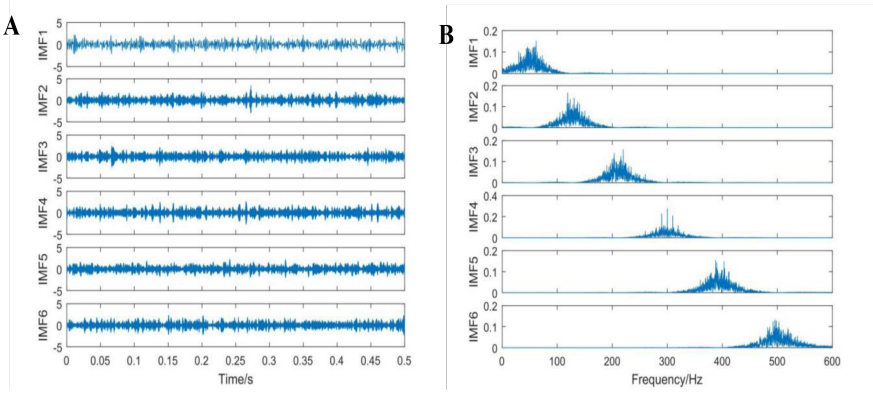

Figure 7. Variational mode decomposition (VMD) results of the simulation signal. (A) Intrinsic mode function (IMF) components obtained from the VMD of the simulated signal. (B) Frequency spectra of the IMF components obtained from the VMD

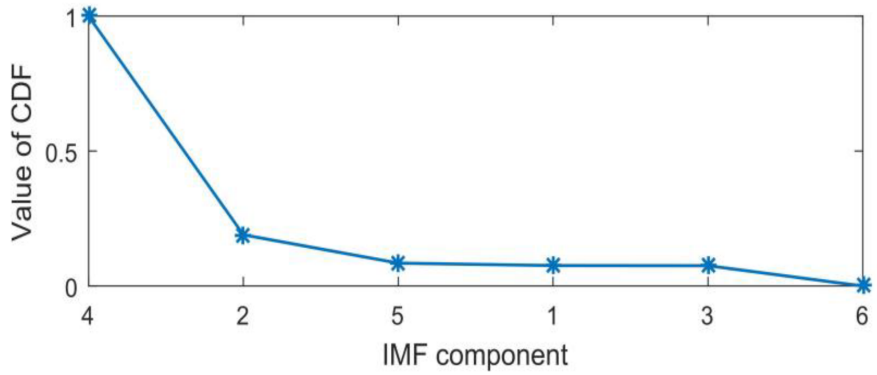

Figure 8. A complete verification of each intrinsic mode function (IMF) component obtained by variational mode decomposition
Abbreviation: CDF: Comprehensive discriminant factor.

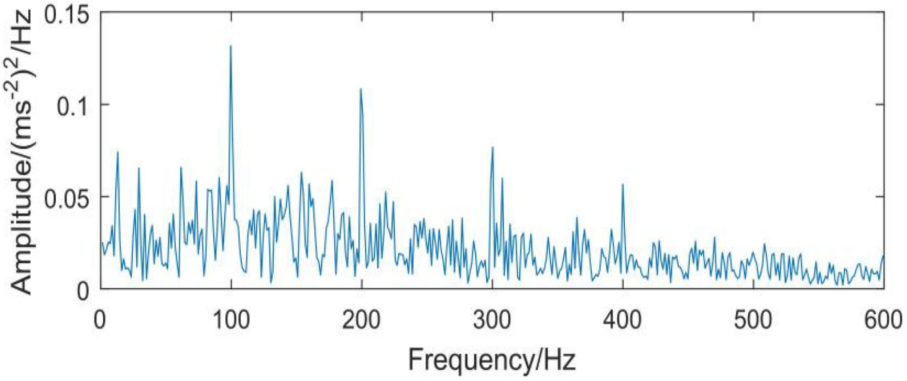

Figure 9. Envelope spectrum of the sensitive component IMF4, obtained from variational mode decomposition

displays the computed envelope spectrum; the remaining IMF components were regarded as iteration error or noise interference components. Accurate fault detection is made possible by the clear identification of the simulated signal's fault frequency and its harmonics in Figure 9.

When the simulation signal $y(t)$ was decomposed using the EMD and EEMD methods, white noise with a standard deviation $\varepsilon_0 = 0.2$ was added to the signal during the EEMD decomposition process, and the total average number of iterations (I) was 100. Following decomposition, the numbers of IMF components obtained from EMD and EEMD are presented in Figures 10 and 11, respectively. To make comparisons easier and to provide clarity, the time-domain waveform and frequency spectra of the first six IMF components are shown in Figures 10 and 11.

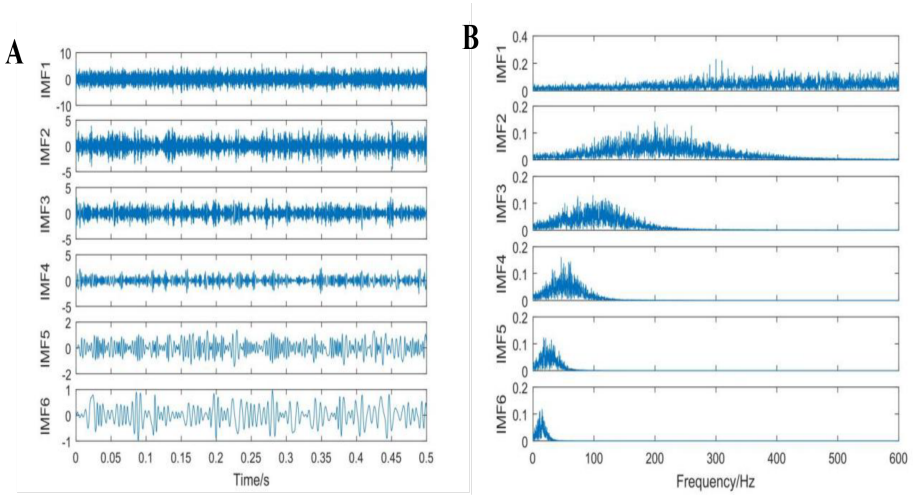

Figure 10. The first six intrinsic mode function (IMF) components (A) and their corresponding frequency spectra (B) obtained from the empirical mode decomposition of the simulated signal

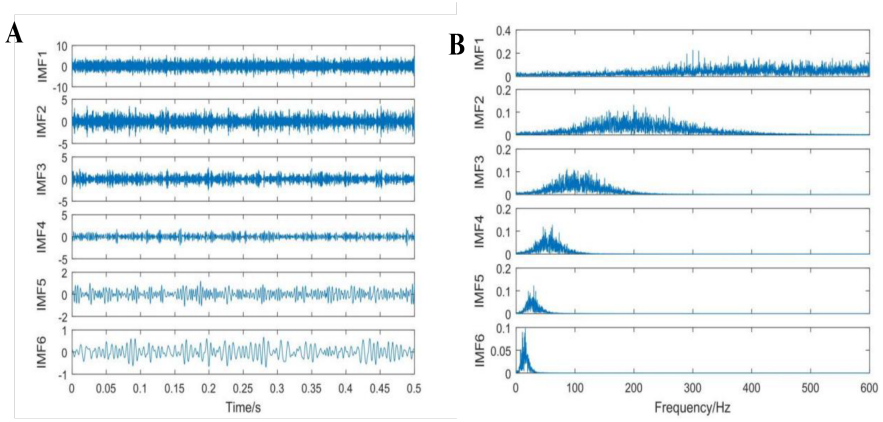

Figure 11. The first six intrinsic mode function (IMF) components (A) and their corresponding frequency spectra (B) obtained from the ensemble empirical mode decomposition of the simulated signal

Comparing the spectra in Figures 7, 10, and 11, it can be observed that the decomposition results of EMD and EEMD are not ideal. The IMF components obtained from both methods exhibit varying degrees of mode mixing, with the IMF1 component being the most significant. The frequency spectrum of IMF1 shows a highly chaotic pattern, with spectral lines scattered across all frequency ranges. This influences the accuracy of the features extracted from the signal.

However, it is necessary to select the IMF components that effectively represent the signal characteristics in EMD and EEMD. The comprehensive evaluation factor for each IMF component was calculated (Figure 12).

The largest difference between EMD and EEMD occurs between IMF1 and IMF2, as seen in Figure 12. Therefore, IMF1 was chosen as the sensitive IMF component, and its envelope was demodulated. Figure 13 presents the resulting envelope spectrum.

As shown in Figure 13, the envelope spectra of the sensitive IMF1 component obtained from EMD and EEMD are both chaotic. Although spectral lines exist at the fault frequency, there are many interference components, and the spectrum does not exhibit regular variations. As a result, the fault frequency could not be accurately identified, and the required valid information was not obtained, thus complicating the fault diagnosis process. The primary reason for this issue is that the EMD method suffers from mode mixing due to its inherent algorithmic limitations. While the EEMD method can address this issue to some extent, the white noise added to the signal cannot be completely neutralized, significantly affecting the accuracy of the decomposition method.

Based on the above analysis, it can be concluded that GJO–VMD can adaptively determine the most suitable key decomposition parameters according to the characteristics of the signal.

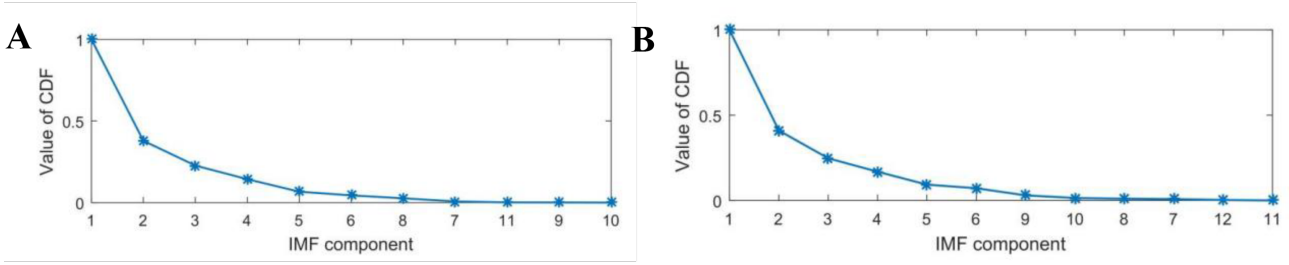

Figure 12. Comprehensive evaluation factors of each intrinsic mode function (IMF) component obtained by empirical mode decomposition (A) and ensemble empirical mode decomposition (B) methods
Abbreviation: CDF: Comprehensive discriminant factor.

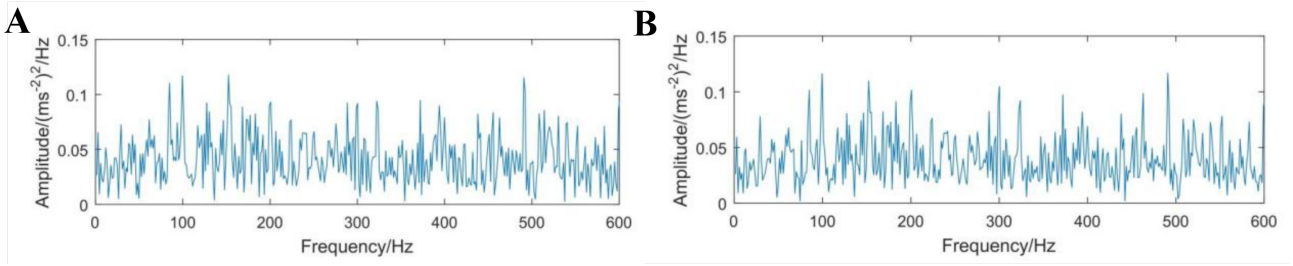

Figure 13. Envelope spectrum of the sensitive IMF1 component obtained from empirical mode decomposition (A) and ensemble empirical mode decomposition (B) methods

Combined with the comprehensive evaluation factor method, it effectively selects the IMF components that are sensitive to signal features, ensuring accurate identification between signals of different states for subsequent analysis.

5. Experimental study

The rolling bearing signal used in the experiment was selected from the bearing dataset supplied by Case Western Reserve University. Data were collected from the vibration test rig, primarily composed of a three-phase induction motor, coupler, accelerometer, encoder, power meter, and other equipment (Figure 14). Figure 15 illustrates an overview of the test rig.

A 6205 2RSJEM bearing (SKF Group, Sweden) was used in the experiment, with the bearing specifications presented in Table 2. At a motor speed of 1797 rpm and a sampling frequency of 12 kHz, the acceleration signal from the bearing at the drive end was recorded. To replicate localized single-point flaws, electrical spark erosion was used to form pits on the test bearing's inner ring, outer ring, and rolling elements, measuring 0.18 mm in diameter and 0.28 mm in depth. Sixty samples, each containing 3000 data points, were gathered for every fault state.

Table 2. Specifications of the rolling bearing

Parameter	Value
Rolling diameter (mm)	8
Pitch diameter (mm)	39
Inner diameter (mm)	25
External diameter (mm)	52
Number of rolling elements	9
Contact angle (°)	0

A randomly selected inner race fault (IRF) signal is presented in Figure 16. This signal exhibits a significant level of noise interference, which can be attributed to the absence of a noise-filtering mechanism in the data acquisition equipment. If the features extracted from this noisy signal are used directly, it becomes difficult to accurately diagnose the rolling bearing's operating condition and fault type. Therefore, noise filtering of the recorded vibration signal is essential to enhance its features.

The IRF signal in Figure 16 was decomposed using the VMD approach. Prior to decomposition, optimization of α and K was required. Using 10 iterations and a population size of 50, the GJO parameter optimization approach was applied. K and α have search spaces that fall between [100, 5000] and [2, 7], respectively. Figure 17 presents the search results. The fitness value steadily declines as the number of iterations rises. After two

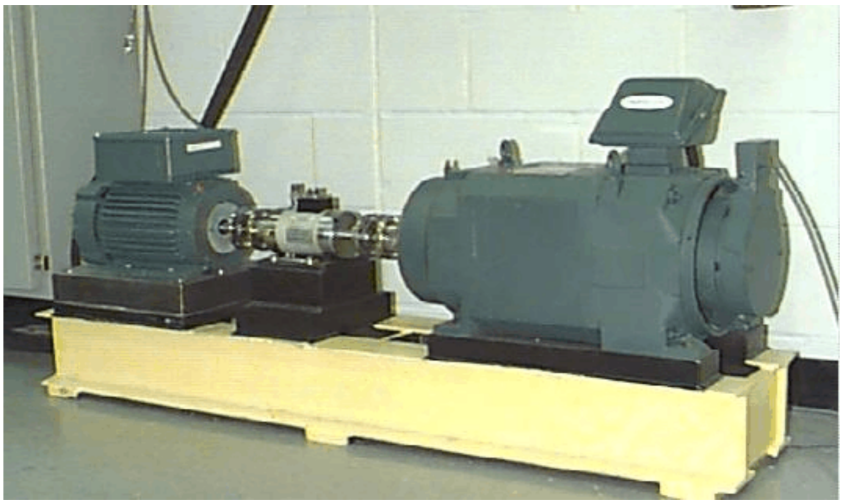

Figure 14. Rolling bearing fault simulation test rig

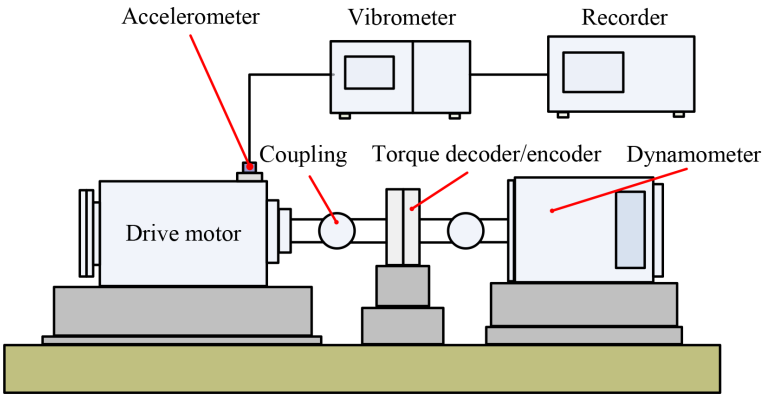

Figure 15. An illustration of the test rig used in the experiment

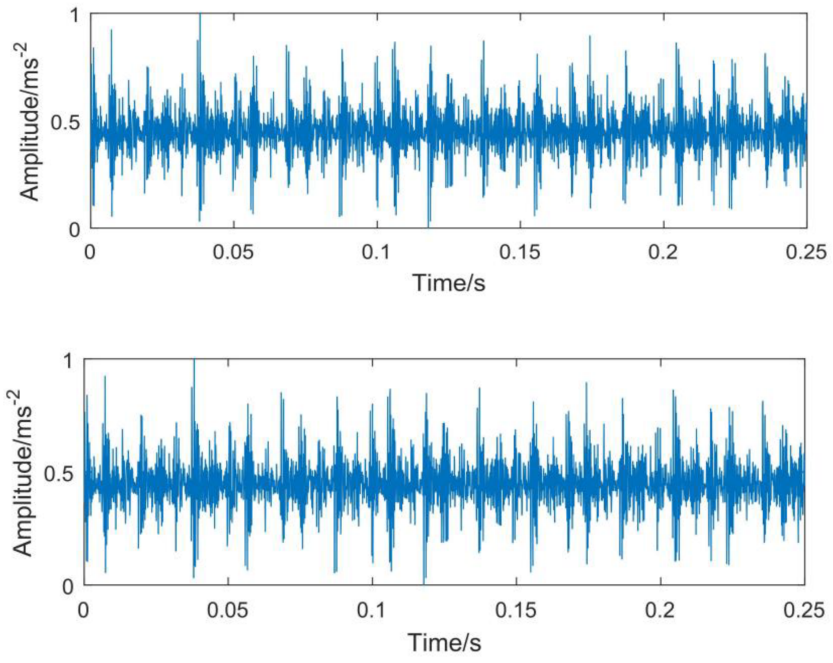

Figure 16. Time-domain waveform of the inner race fault signal

iterations, the ideal parameters were determined, with K and α values of (5, 550).

Figure 18 demonstrates the IMF components and their frequency spectra after the IRF signal

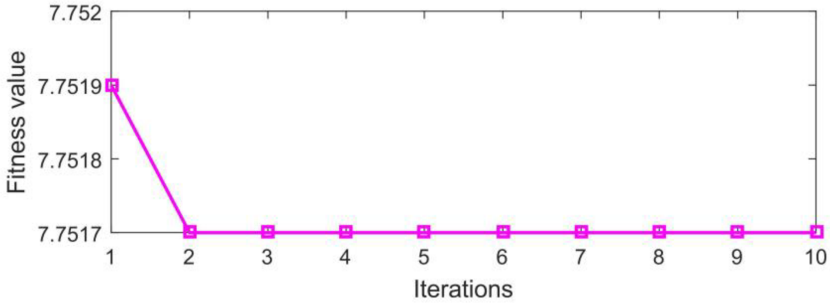

Figure 17. Fitness iteration curve for inner race fault signal

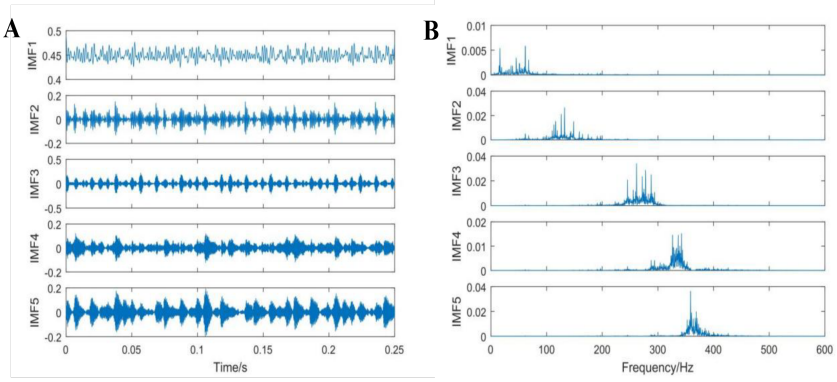

Figure 18. Intrinsic mode function (IMF) components (A) and their frequency spectra (B) obtained from the golden jackal optimization–variational mode decomposition of the inner race fault signal

was decomposed using the ideal parameters. Each IMF component was focused around its center frequency, as shown in Figure 18B, with no frequency overlap. This result suggests that the decomposition parameters selected were appropriate and successfully addressed the issue of modal aliasing. As seen in Figure 19, by calculating the complete assessment factors of each IMF component, the sensitive IMF component containing IRF feature information could be easily identified.

As shown in Figure 19, the largest difference in the comprehensive evaluation factors occurs between IMF1 and IMF2. Consequently, IMF**X** was identified as the sensitive component, and its corresponding signal was reconstructed (Figure 20).

By comparing the signals in Figures 16 and 20, it is evident that the signal's impact characteristics have become more prominent and that the noise components have been successfully filtered. These impact features represent fault-characteristic data that was previously obscured by noise. Using the previously described procedures, the normal, outer race fault, and rolling element fault signals were reconstructed. Table 3 summarizes the key decomposition parameters for the GJO–VMD.

Table 3. Key decomposition parameters for the golden jackal optimization–variational mode decomposition method

Rolling bearing condition	**Key parameters**	
	K	α
Normal	3	2796
REF	6	2970
ORF	4	1259

Abbreviations: ORF, outer race fault; REF, rolling element fault.

The MFE values of the reconstructed signals were calculated, and a randomly selected set of MFE curves for rolling bearing signals under different states are presented in Figure 21. Due to the elimination of interference factors, these MFE values exhibit excellent overall distinguishability despite some overlaps occurring at certain scale factors. This result indicates that, following the GJO–VMD and the elimination of the IMF false parts, noise interference and other irrelevant features of the signals were effectively suppressed. As a result, the similarity between signals from different states was reduced, and the signal state characteristics were effectively highlighted. The MFE values of the signals, after the GJO–VMD and reconstruction, are used to construct state feature vectors, which serve as the diagnostic basis

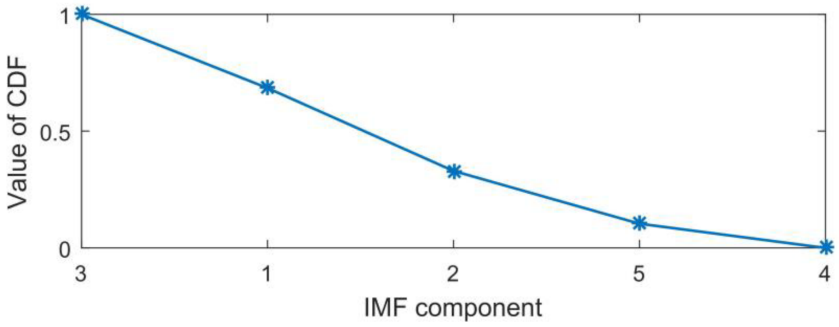

Figure 19. Comprehensive evaluation factors of the intrinsic mode function (IMF) components obtained from the golden jackal optimization–variational mode decomposition
Abbreviation: CDF: Comprehensive discriminant factor.

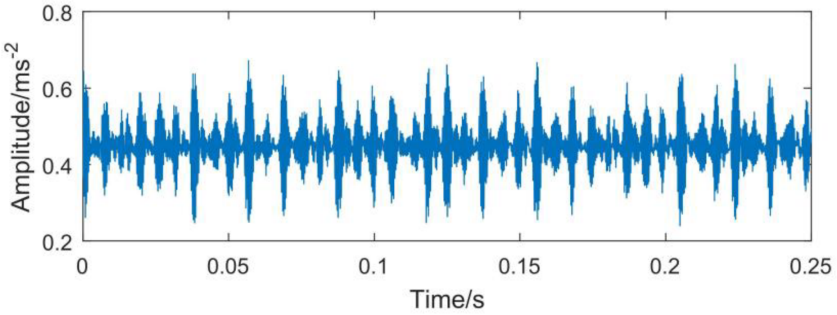

Figure 20. Reconstructed signal of the inner race fault

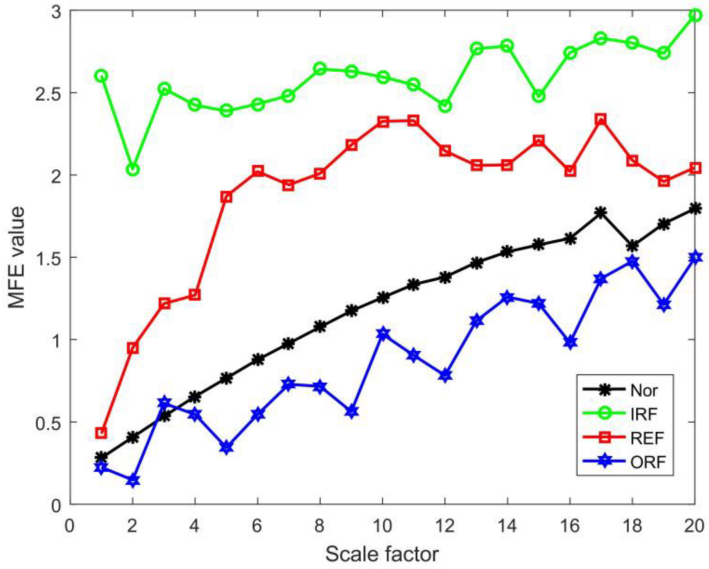

Figure 21. Multiscale fuzzy entropy (MFE) curves of reconstructed signals for rolling bearings under different states
Abbreviations: IRF: Inner race fault; Nor: Normal; ORF: Outer race fault; REF: Rolling element fault.

for determining the working condition of rolling bearings.

A maximum of 1000 iterations was set for network training, with a learning rate of 0.01 and a target minimum error of 0.0001. Forty state feature vectors from each condition of the rolling bearings were randomly chosen as training samples to train the classifier; the state feature vectors were used as testing samples to assess the classifier's performance. The fitness function was the sum of the error rates for the training and testing sets. The GSABO population was set at 50, with a chaotic coefficient of 2, a maximum of 10 iterations, and threshold weight limits of [−3,

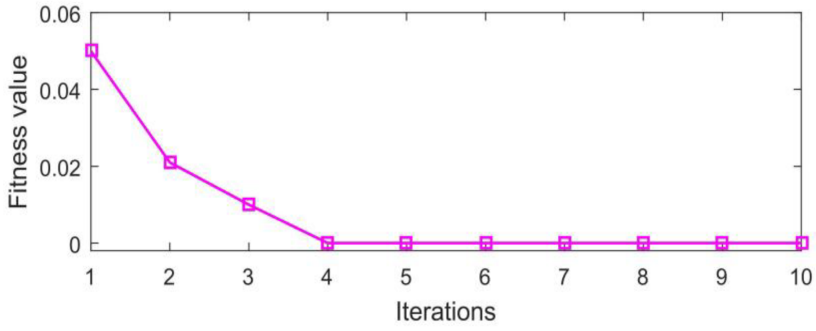

Figure 22. Fitness curve of the golden sine subtraction-average-based optimizer.

3]. The BP neural network's initial thresholds and weights were both set to 1. Figure 22 illustrates the resulting fitness curve.

The ideal value was discovered following four GSABO repetitions, as illustrated in Figure 22. The threshold value was 0.92, while the optimum weights for the BP neural network were 1.08. The K-nearest neighbor (KNN), support vector machine (SVM), random forest, decision tree, and BP neural network classifiers were used to compare the classification efficacy of the GSABO–BP neural network. This allows the effectiveness of each classification method to be validated. The Euclidean distance served as the distance metric between samples in the KNN classifier. A grid search approach was employed to determine the optimal k value. The model was trained using multiple values: $\{3, 5, 7, 9, 11, 13\}$, and three-fold cross-validation was used to evaluate performance for each setting. A decision tree classifier was used, with entropy selected as the splitting parameter.

In the planning and design of gardens or nature reserves, efforts should be made to ensure that the tree density is appropriate and that the maximum rooting depth—the deepest extent tree roots can reach—is maximized within the boundaries of ecology and geography. This approach enhances ecosystem stability, improves soil and water conservation, and promotes biodiversity. In the random forest classifier, the number of trees and the maximum depth of the trees are optimized using the grid search method within the ranges of $\{120, 200, 300\}$ and $\{5, 8, 15\}$, respectively. At the same time, 3-fold cross-validation is combined to evaluate the performance of each parameter combination, thereby selecting the best parameters. The parameters of the SVM and BP neural network are set to default values, and the SVM kernel function is set to the linear kernel function. Each classifier is run five times, and the average value of the five runs is taken as the final diagnostic result. The results are shown in Table 4.

Table 4. Fault diagnosis accuracy of different classification methods

Methods	Accuracy rate (%)
KNN	98.75
SVM	99.38
Random forest	99.07
Decision tree	97.50
BP neural network	97.33
GSABO–BP neural network	100.00

Abbreviations: BP: Back propagation; GSABO: Golden sine subtraction-average-based optimizer; KNN: K-nearest neighbor; SVM: Support vector machine; SVM: Support vector machine.

As indicated in Table 4, all classification approaches exhibited varying degrees of misdiagnosis, except for the GSABO–BP neural network, which reached a 100% diagnosis accuracy. This discrepancy is primarily attributed to the small number of training samples. Classifiers such as KNN, SVM, random forest, decision tree, and BP neural network require larger datasets to ensure robust performance and generalization. In contrast, the classification performance and diagnosis accuracy are markedly enhanced by the GSABO–BP neural network with the optimal network parameters.

To further verify the accuracy and robustness of the GSABO–BP neural network, all classification methods were tested using training sample sizes ranging from 10 to 50, and testing sample sizes decreased correspondingly from 50 to 10. For each method, the average diagnostic accuracy over five runs was calculated and used as the evaluation metric. The results are summarized in Table 5.

Table 5 illustrates how the diagnostic accuracy of all approaches steadily increases as the

Table 5. Diagnostic accuracy of various classification methods under different conditions

Classification method	Diagnostic accuracy under varying testing sample sizes (%)				
	50 (10)	40 (20)	30 (30)	20 (40)	10 (50)
KNN	93.50	96.25	99.17	98.75	100.00
SVM	97.50	97.50	99.38	99.38	100.00
Random forest	97.00	97.50	98.00	99.07	99.38
Decision tree	96.00	96.25	97.50	97.50	100.00
BP neural network	84.50	95.63	97.50	97.33	97.50
GSABO–BP neural network	99.00	100.00	100.00	100.00	100.00

Note: ( ) represents the number of training samples.
Abbreviations: BP: Back propagation; GSABO: Golden sine subtraction-average-based optimizer; KNN: K-nearest neighbor; SVM: Support vector machine.

number of training samples rises. In all cases, the GSABO–BP neural network achieved 100% diagnostic accuracy, except in the scenario with 50 testing samples and 10 training samples, where misclassification took place. In contrast, other approaches exhibit misdiagnoses due to limitations in training sample size and the configuration of associated parameters. These results highlight that the proposed fault diagnostic approach, based on GJO–VMD, MFE, and GSABO–BP neural network, is capable of achieving optimal diagnostic performance even under limited training sample conditions.

Additionally, the validity of the GJO–VMD method is demonstrated by comparing it with signal decomposition methods such as EMD or EEMD. The comprehensive evaluation factor technique was used to reconstruct signals, and the state feature vectors were created by calculating the MFE values of the reconstructed signals. The GSABO–BP neural network's diagnostic results, averaged over five trials, are presented in Table 6 based on various signal decomposition techniques.

As indicated in Table 6, the diagnostic accuracy based on the GJO–VMD approach achieved 100% in all circumstances, except in the scenario with 50 test samples and 10 training samples, where misdiagnosis took place. This suggests that the proposed approach is capable of efficiently removing a signal's interference components and obtaining IMF components that are responsive to the signal features—these components are then utilized for feature extraction. Conversely, under various test sample settings, the EMD and EEMD techniques showed differing degrees of misclassification. Compared to GJO–VMD, the overall diagnostic accuracy was lower. This is primarily because the EMD approach experiences modal aliasing during signal decomposition, which compromises decomposition accuracy and prevents the complete elimination of interference components. Although EEMD can effectively suppress modal aliasing by adding white noise, it is unable to fully remove the introduced noise, resulting in higher similarity in MFE values between signals of different states. Consequently, this leads to reduced diagnostic accuracy.

6. Conclusion

To address the challenges of extracting fault features from rolling bearings and the unsatisfactory diagnostic performance of conventional classification models under small-sample size conditions, this study proposes a fault diagnosis method that integrates GJO–VMD and MFE with a GSABO–BP neural network.

Through the analysis of both simulated and real-world rolling bearing fault signals, as well as comparative evaluation against traditional approaches, the following conclusions are drawn:

- The signal processing method based on GJO–VMD, combined with the comprehensive evaluation factor strategy, effectively decomposes nonlinear and non-stationary signals, determining IMF components that are sensitive to fault characteristics. This approach successfully suppresses background noise, environmental interference, and irrelevant components. Compared to EMD and EEMD, the GJO–VMD method offers more accurate and meaningful signal decomposition, thereby ensuring the reliable extraction of fault features.
- The MFE curves derived from GJO–VMD-reconstructed signals can effectively capture the characteristic differences among various rolling bearing operating states. When coupled with the GSABO–BP neural network, this approach achieves reliable fault diagnosis performance even in scenarios with limited sample sizes.
- The GSABO–BP neural network, once optimized, demonstrates robust parameter selection. Except for a single misclassification at the 50-sample level, it achieves a diagnostic accuracy of 100% for all other test sample sizes

Table 6. Diagnostic accuracy of different signal decomposition methods under varying conditions

Signal decomposition method	Diagnostic accuracy under varying testing sample sizes (%)				
	50 (10)	**40 (20)**	**30 (30)**	**20 (40)**	**10 (50)**
EMD	95.50	96.88	96.67	98.75	100.00
EEMD	88.00	86.67	85.56	86.67	93.33
GJO–VMD	99.00	100.00	100.00	100.00	100.00

Note: ( ) represents the number of training samples.
Abbreviations: EEMD: Ensemble empirical mode decomposition; EMD: Empirical mode decomposition; GJO–VMD: Golden jackal optimization–variational mode decomposition.

ranging from 40 to 10. Compared with other commonly used classifiers, such as KNN, SVM, random forest, decision tree, and standard BP neural networks, the proposed method exhibits superior diagnostic accuracy and robustness.

In this study, the rolling bearing vibration signals were investigated. It is anticipated that the proposed method will also perform well when applied to other signals. In future work, this method should be extended from rolling bearings to other types of rotating machinery, such as gears and rotors, to enhance the universality of diagnosis. At the same time, by integrating the method with real-time monitoring systems, it will be possible to develop fault diagnosis technologies suitable for online monitoring, thereby addressing the growing demand for real-time monitoring and rapid diagnosis in industrial applications.

Acknowledgments

None.

Funding

None.

Conflict of interest

The authors declare they have no competing interests.

Author contributions

Conceptualization: Zhang Jing Song, Zhou Xiao Long
Investigation: Zhang Jing Song, Wang Yan Zhen
Methodology: Zhou Xiao Long, Zheng Bin
Formal analysis: Jing Zhe, Li Hao Yu
Writing – original draft: Zhang Jing Song
Writing – review & editing: Zhang Jing Song, Zhou Xiao Long, Yang Soo Sing, Tan Min Keng

Availability of data

The raw data supporting the findings of this study are available at https://github.com/yyxyz/CaseWesternReserveUniversityData.

AI tools statement

All authors confirm that no AI tools were used in the preparation of this manuscript.

References

1. Song X, Wang H, Liu Y, Wang Z, Cui Y. A fault diagnosis method of rolling element bearing based on improved PSO and BP neural network. *J Intell Fuzzy Syst.* 2022;43(5):5965-5971 https://doi.org/10.3233/JIFS-213485
2. Hu R, Zhang M, Xiang Z, Mo J. Guided deep subdomain adaptation network for fault diagnosis of different types of rolling bearings. *J Intell Manuf.* 2023;34(5):2225-2240 https://doi.org/10.1007/s10845-022-01910-7
3. Lei Y, Li N, Guo L, Li N, Yan T, Lin J. Machinery health prognostics: a systematic review from data acquisition to RUL prediction. *Mech Syst Signal Process.* 2018;104:799-834 https://doi.org/10.1016/j.ymssp.2017.11.016
4. Liu R, Yang B, Zio E, Chen X. Artificial intelligence for fault diagnosis of rotating machinery: A review. *Mech Syst Signal Process.* 2018;108:33-47 https://doi.org/10.1016/j.ymssp.2018.02.016
5. Zhou Y, Jin Z, Zhang Z, Geng Z, Zhou L. Adversarial subdomain adaptation method based on multi-scale features for bearing fault diagnosis. *Math Found Comput.* 2024;7(4):485-511 https://doi.org/10.3934/mfc.2023024
6. Kanneg D, Wang W. A wavelet spectrum technique for machinery fault diagnosis. *J Signal Inf Process.* 2011;2(4):322-329 https://doi.org/10.4236/jsip.2011.24046
7. Feng H, Chen R, Wang Y. Feature extraction for fault diagnosis based on wavelet packet decomposition: An application on linear rolling guide. *Adv Mech Eng.* 2018;10(8):1687814018796367 https://doi.org/10.1177/1687814018796367
8. Zhou X, Wang X, Wang H, et al. Method for denoising the vibration signal of rotating machinery through VMD and MODWPT. *Sensors (Basel).* 2023;23(15):6904 https://doi.org/10.3390/s23156904
9. Huang NE, Shen Z, Long SR, et al. The empirical mode decomposition and the Hilbert spectrum for nonlinear and non-stationary time series analysis. *Proc R Soc Lond A Math Phys Eng Sci.*

1998;454(1971):903-995
https://doi.org/10.1098/rspa.1998.0193
10. Wu Z, Huang NE. Ensemble empirical mode decomposition: a noise-assisted data analysis method. *Adv Adapt Data Anal.* 2009;1(01):1-41
https://doi.org/10.1142/S1793536909000047
11. Zhou H, Jia M. EMD Hilbert [Analysis of rolling bearing fault diagnosis based on EMD and kurtosis Hilbert envelope demodulation]. *Mechatron Eng.* 2014;31(9)
https://doi.org/10.3969/j.issn.1001-4551.2014.09.008
12. Yao F, Yang X, Ding F, Zhao M, Li S. EMD-AR [Fault diagnosis of rolling bearings based on wavelet threshold denoising, EMD-AR spectrum analysis, and extreme learning machine]. *, [Manuf Technol Mach Tool.]* 2023;(7):16-20
https://doi.org/10.19287/j.mtmt.1005-2402.2023.07.002
13. Qin YF, Fu X, Li XK, Li HJ. ADAMS simulation and HHT feature extraction method for bearing faults of coal shearer. *Processes.* 2024;12(1):164
https://doi.org/10.3390/pr12010164
14. Zhang F, Gao S, Zhang W, Li G. Improved EEMD and overlapping group sparse second-order total variation. *J Braz Soc Mech Sci Eng.* 2024;46(6):386
https://doi.org/10.1007/s40430-024-04965-0
15. Damine Y, Bessous N, Pusca R, et al. A new bearing fault detection strategy based on combined modes ensemble empirical mode decomposition, KMAD, and an enhanced deconvolution process. *Energies.* 2023;16(6):2604
https://doi.org/10.3390/en16062604
16. Zhou X, Wang X, Wang H, et al. Rotor fault diagnosis method based on VMD symmetrical polar image and fuzzy neural network. *Appl Sci (Basel).* 2023;13(2):1134
https://doi.org/10.3390/app13021134
17. Dragomiretskiy K, Zosso D. Variational mode decomposition. *IEEE Trans Signal Process.* 2014;62(1-4):531-544
https://doi.org/10.1109/TSP.2013.2288675
18. Wei W, He G, Yang J, Li G, Ding S. Tool wear monitoring based on the gray wolf optimized variational mode decomposition algorithm and Hilbert–Huang transformation in machining stainless steel. *Machines.* 2023;11(8):806
https://doi.org/10.3390/machines11080806
19. Meraihi Y, Gabis AB, Mirjalili S, Ramdane-Cherif A. Grasshopper optimization algorithm: theory, variants, and applications. *IEEE Access.* 2021;9:50001-50024
https://doi.org/10.1109/ACCESS.2021.3067597
20. Gandomi AH, Yang XS, Alavi AH. Cuckoo search algorithm: a metaheuristic approach to solve structural optimization problems. *Eng Comput.* 2013;29:17-35
https://doi.org/10.1007/s00366-011-0241-y
21. Chopra N, Ansari MM. Golden jackal optimization: a novel nature-inspired optimizer for engineering applications. *Expert Syst Appl.* 2022;198:116924
https://doi.org/10.1016/j.eswa.2022.116924
22. Chai X, Liu W. CEEMDAN [Gas valve fault diagnosis based on improved CEEMDAN and multi-scale fuzzy entropy]. *[Mod Mach Tool Manuf Technol.]* 2020 ;(10):140-143
https://doi.org/10.13462/j.cnki.mmtamt.2020.10.033
23. Huang Z, Xie Y. Fault diagnosis method of rolling bearing based on BP neural network. In: *2009 International Conference on Measuring Technology and Mechatronics Automation.* Vol 1. IEEE; 2009:647-649
https://doi.org/10.1109/ICMTMA.2009.246
24. Chen G, Lu X, Liu T. [Rolling bearing fault diagnosis based on BWO-optimized VMD and singular spectrum entropy]. . *[Equip Manuf Technol.]* 2023. https://www.fx361.com/page/2023/1124/22807868.shtml
25. Shan YT, Liu T, Chu W, et al. [Application of genetic algorithm-optimized variational mode decomposition in bearing fault feature extraction]. *[Noise Vib Control.]* 2024;44(1):148-153.
https://nvc.sjtu.edu.cn/CN/Y2024/V44/I1/148
26. Zhou X, Zhang Y, Wang Y, Ma F. VMD AR [Application of VMD-based AR mode and correlation dimension in fault feature extraction for gear]. *Manuf Technol Mach Tool.* 2021;(1):91-95.
27. Zahid M, Ud Din F, Shah K, Abdeljawad T. Fuzzy fixed point approach to study the existence of solution for Volterra type integral equations using fuzzy Sehgal contraction. *PLoS One.* 2024;19(6):e0303642
https://doi.org/10.1371/journal.pone.0303642
28. Trojovský P, Dehghani M. Subtraction-average-based optimizer: a new swarm-inspired metaheuristic algorithm for solving optimization problems. *Biomimetics.* 2023;8(2):149
https://doi.org/10.3390/biomimetics8020149
29. Antoni J, Randall RB. The spectral kurtosis: application to the vibratory surveillance and diagnostics of rotating machines. *Mech Syst Signal Process.* 2006;20(2):308-331
https://doi.org/10.1016/j.ymssp.2004.09.002

Jingsong Zhang *is a current master's student at the Engineering College of Sabah University in Malaysia.*
https://orcid.org/0009-0001-6397-3454

Xiaolong Zhou *is a vice dean and associate professor of the Mechanical Engineering College of Beihua University. He has a high level of academic expertise in the fields of mechanical engineering and control engineering.*
https://orcid.org/0000-0002-0934-6046

Soo Siang Yang*is is an associate professor of the Engineering College at Universiti Malaysia Sabah.*

Min Keng Tan *is currently a senior lecturer with the Faculty of Engineering, Universiti Malaysia Sabah. His research interests include multiagent systems, computational intelligence, and smart energy.Min Keng Tan received the B.Eng. (Hons.), M.Eng. and Ph.D. degrees in Electrical and Electronic Engineering from Universiti Malaysia Sabah, Malaysia.*
https://orcid.org/0000-0003-4420-186X

Yanzhen Wang *is a current master's student at the School of Mechanical Engineering of Beihua University.*
https://orcid.org/0009-0005-2536-7145

Bin Zheng *is a current master's student at the Engineering College of Sabah University in Malaysia.*
https://orcid.org/0009-0006-6334-0231

Jing Zhe *is a current undergraduate student studying in the Department of Mechanical Engineering at Beihua University.*
https://orcid.org/0009-0001-5380-0197

Haoyu Li *is a current undergraduate student studying in the Department of Mechanical Engineering at Beihua University.*
https://orcid.org/0009-0001-6668-0040

An International Journal of Optimization and Control: Theories & Applications
(https://accscience.com/journal/ijocta)